Hindawi
Complexity
Volume 2020, Article ID 8814460, 10 pages
https://doi.org/10.1155/2020/8814460

Research Article

Disturbance-Observer-Based Fuzzy Control for a Robot Manipulator Using an EMG-Driven Neuromusculoskeletal Model

Longbin Zhang[1], **Wen Qi**[2], **Yingbai Hu**[3] and **Yue Chen**[4]

[1]*Department of Engineering Mechanics, KTH Royal Institute of Technology, SE-100 44 Stockholm, Sweden*
[2]*Dipartimento Di Elettronica, Informazione e Bioingegneria, Politecnico Di Milano, 20133 Milano, Italy*
[3]*Department of Informatics, Technical University of Munich, Munich 85748, Germany*
[4]*Department of Mechanical Engineering, University of Arkansas, Fayetteville 72701, AR, USA*

Correspondence should be addressed to Longbin Zhang; longbin@kth.se

Received 18 September 2020; Revised 1 November 2020; Accepted 17 November 2020; Published 30 November 2020

Academic Editor: Ning Wang

Robot manipulators have been extensively used in complex environments to complete diverse tasks. The teleoperation control based on human-like adaptivity in the robot manipulator is a growing and challenging field. This paper developed a disturbance-observer-based fuzzy control framework for a robot manipulator using an electromyography- (EMG-) driven neuromusculoskeletal (NMS) model. The motion intention (desired torque) was estimated by the EMG-driven NMS model with EMG signals and joint angles from the user. The desired torque was transmitted into the desired velocity for the robot manipulator system through an admittance filter. In the robot manipulator system, a fuzzy logic system, utilizing an integral Lyapunov function, was applied for robot manipulator systems subject to model uncertainties and external disturbances. To compensate for the external disturbances, fuzzy approximation errors, and nonlinear dynamics, a disturbance observer was integrated into the controller. The developed control algorithm was validated with a 2-DOFs robot manipulator in simulation. The results indicate the proposed control framework is effective and crucial for the applications in robot manipulator control.

1. Introduction

Robotic manipulators are increasingly used in welding automation, robotic surgery [1], and space, as they are able to complete diverse tasks in complex environments, such as uncertain system dynamics, time-vary delays, and unknown external disturbances. The robot manipulator may work within dangerous environments for unfriendly tasks, such as handing radioactive material and searching, and the teleoperation control of the robot manipulator has been widely utilized into the controller design. Yang et al. [2] proposed an admittance-adaptation-based methodology for robot manipulators when interacting with unknown environments and guaranteed trajectory tracking performance. Recently, there is a growing demand for the natural interface between the robotic manipulator and the user [3]. Specifically, the robotic manipulator is teleoperated by the user with human-like characteristics. A human-like learning controller was proposed to optimally adapt interaction with unknown environments [4], and the human-like adaptivity was shown well by the robot manipulator in stable and unstable tasks.

The development of robot manipulator controller with human-like characteristics (the user's intention) requires accurate and robust decoding of motor function. Muscle electromyographic (EMG) signals from the central nervous system (CNS) [5, 6] are widely used in the user's intention detection as EMG signals are relatively easy to acquire and process and provide essential information on human motion. EMG-based modelling methodologies have been utilized into various human-machine control algorithms for robot manipulators. Ryu et al. [7] developed a continuous position-based strategy for a robot manipulator with EMG signals and the manipulator could replicate the movements from the user well, thereby improving the control strategy

for teleoperated robot manipulators. Artemiadis et al. [3] proposed a teleportation methodology for a robot manipulator based on EMG signals and position feedback and realized a good master-slave manipulator system with human-like adaptivity. Bu et al. [8] proposed a Bayesian-network-based model to predict occurrence probabilities of the motions with the given information of the previous motion and classify hybrid motions with EMG signals. Their results demonstrated that the EMG-based Bayesian network model could improve the robustness and stability for motion classification. Therefore, integrating an EMG-driven neuromusculoskeletal (NMS) model with human-like characteristics into the robot manipulator controller is valuable and could be crucial in the robot manipulator control field [9].

Diverse control strategies for robot manipulators have been developed in complex environments [10–12], as these environments could degrade the performance of the robot manipulator system [13, 14]. Lin et al. [15] developed fuzzy Gaussian mixture models to approximate the objects' shape for robot manipulator grasping tasks under unknown environments, and the model has a good grasp quality. He et al. [16] proposed a disturbance-observer-based control strategy to approximate unknown parameters and disturbance for multimanipulator robots and validated on a dual-arm cooperative robot (Baxter). Their results showed that the controller has an accurate control performance and was able to compensate for the errors due to the model uncertainties and external disturbances. Yang et al. [17] proposed a disturbance-observer-based impedance control for uncertain robot manipulators in unknown environments. Fuzzy logic system and disturbance observer are two commonly used techniques in the control system to compensate for unknown functions, parameters, and disturbance [18–20]. Therefore, in this study, a disturbance-observer-based fuzzy algorithm was integrated into the control framework for a robot manipulator, subjected to practical problems including external disturbances and model uncertainties.

The objective of this study was to design a disturbance-observer-based fuzzy controller for a 2-DOFs robot manipulator using an EMG-driven NMS model. The main contributions of this paper are as follows: (1) a disturbance-observer-based fuzzy control framework is developed that fully incorporates a robot manipulator system with an EMG-driven NMS model and could be applied in controlling the movement of robot manipulators with human-like characteristics; (2) the user's motion intention was able to be well-predicted by the EMG-driven model and transmitted into the desired velocity through an admittance filter, which allows the robot manipulator system behave with human-like adaptivity; (3) in the current paper, the control framework we proposed in general is useful for obtaining the human-like characteristics, as well as simulating the control strategy in the robot manipulator system, and thus be of large benefit for teleoperation robot manipulator applications.

2. Methods

2.1. Controller Framework. A disturbance-observer-based fuzzy control framework (Figure 1) was developed for a robot manipulator system in complex environments. In the robot manipulator controller design, to complete tasks with human-like characteristics, an EMG-driven NMS model through the EMG signals and joint angles from the user was used to estimate the desired torque. The desired torque was transmitted into the desired velocity through an admittance filter. A disturbance-observer-based adaptive controller with fuzzy compensation was developed for the robot manipulator with unknown model dynamics.

2.2. EMG-Driven Neuromusculoskeletal Model. A previously developed EMG-driven NMS model [21] was used in this study. It reproduces the transformations from EMG signal generation and joint angles to musculotendon forces and joint torques. The NMS model consists of four components: musculotendon kinematics, muscle contraction dynamics, muscle activation dynamics, and joint dynamics [22].

The musculotendon kinematics component used the 3D joint angles to calculate musculotendon lengths and moment arms of individual musculotendon units (MTUs) through a musculoskeletal model. The muscle activation dynamics component calculated muscle activation based on filtered EMG signals. The relation between neural activation $u(t)$ and filtered EMG signal $e(t)$ was represented by a recursive filter [23] as shown in the following equation:

$$u_i(t) = \mu e_i(t-d) - \beta_1 u_i(t-1) - \beta_2 u_i(t-2), \quad (1)$$

where $e_i(t)$ is the linear envelope of the EMG signal of i^{th} muscle; $u_i(t)$ is the neural activation of i^{th} muscle; d is the electromechanical delay; μ is the muscle gain coefficient; and β_1 and β_2 are the recursive coefficients and are subject to the following constraints to obtain a stable solution [21, 23, 24]: $\beta_1 = C_1 + C_2$, $\beta_2 = C_1 \cdot C_2$, where $|C_1| < 1$, $|C_2| < 1$, and $\mu - \beta_1 - \beta_2 = 1$.

The relationship from neural activation to muscle activation is nonlinear and was formulated to describe muscle activation dynamics as follows:

$$a_i(t) = \frac{e^{A_i u_i(t)} - 1}{e^{A_i} - 1}, \quad (2)$$

where $a_i(t)$ is the i^{th} muscle activation and A_i is the nonlinear shape factor of i^{th} muscle and subjected to the interval $(-3, 0)$ with zero representing a linear relationship and negative values introduce a nonlinear relationship [24, 25].

Musculotendon forces were computed through muscle contraction dynamics, based on a 3-element Hill-type muscle model; a series elastic element (SE), a contractile element (CE), and a parallel elastic element (PE). Each MTU's force (F^{mt}) could be represented as a function of

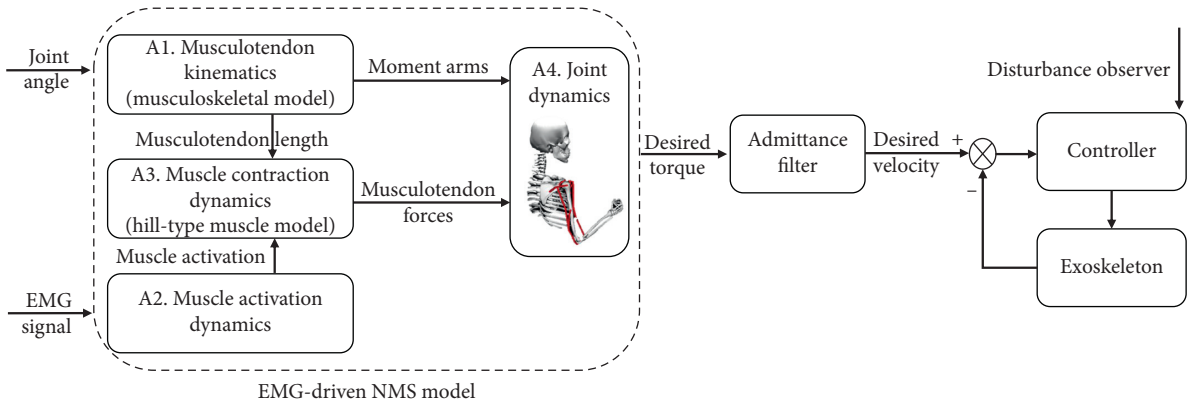

Figure 1: Schematic structure of the controller framework based on an EMG-driven NMS model. The NMS model consists of four components: (A1) the model's musculotendon kinematics were used to compute musculotendon lengths and moment arms; (A2) muscle activation dynamics were employed to calculate the level of muscle activation involved in the processed EMG signals; (A3) muscle contraction dynamics according to a Hill-type muscle model were applied to predict musculotendon force, using calculated musculotendon length and muscle activation as inputs; (A4) joint dynamics was used to compute joint torques, using the calculated musculotendon forces and moment arms as inputs. The EMG signals and joint angles from the user were used to estimate the motion intention (desired torque) through the EMG-driven NMS model. Then, the desired torque was transmitted to the desired velocity through an admittance filter. A disturbance-observer-based adaptive fuzzy controller was developed for the robot manipulator system with model uncertainties.

muscle activation and muscle kinematics as shown in the following equation:

$$F^{\mathrm{mt}} = F_0^m \left[f_a\left(\widetilde{l}_m\right) \cdot f_v\left(\widetilde{v}_m\right) \cdot a + f_p\left(\widetilde{l}_m\right) + d_m \widetilde{v}_m \right] \cos\left(\phi\right), \tag{3}$$

where F_0^m is the maximum isometric muscle force; $f_a(\widetilde{l}_m)$ is the active force-length relationship that describes the ability of muscle fibres to generate forces at different lengths; $\widetilde{l}_m$ is the fibre length normalized with the optimal fibre length; $f_v(\widetilde{v}_m)$ is the force-velocity relationship that represents the muscle fibre force contribution of the fibres' contraction velocity ($\widetilde{v}_m$), and the velocity was normalized with maximum contraction velocity and optimal fibre length; $f_p(\widetilde{l}_m)$ is the passive force-length relationship that expresses the force response to the fibres to strain; d_m is the muscle damping coefficient which represents the muscle damping characteristics; and ϕ is the pennation angle of the fibres.

Joint torques were then estimated by the product of musculotendon forces F_{mt} and moment arms r_{mt} through the joint dynamics component as shown in the following equation:

$$M = r_{\mathrm{mt}} \times F^{\mathrm{mt}}. \tag{4}$$

2.3. Admittance Filter. To control the robot manipulator based on the user's adaptivity (desired torque estimated from EMG signals), an admittance filter was used to transform the joint torque into the desired angular velocity [26, 27].

$$\frac{\Delta\tau(s)}{Ms^2 + Bs + K} = \Delta q(s), \tag{5}$$

where $\Delta\tau$ and Δq are the torque and position regulation and M, B and K are the mass, damping, and stiffness parameters of the admittance filter, respectively.

2.4. Robot Manipulator Dynamic Modelling. The dynamics of a robot manipulator was generally modeled as follows [28]:

$$M(q)\ddot{q} + C(q,\dot{q})\dot{q} + G(q) + f_{\mathrm{dis}} = \tau, \tag{6}$$

where $M(q)$ is inertial matrix; q is the joint angle; $C(q,\dot{q})$ is centripetal and Coriolis force; $G(q)$ is the gravitational force; τ is the joint torque; and f_{dis} is the unknown disturbance.

We rewrite this robot manipulator dynamics as follows:

$$\begin{cases} \mathbf{y} = \mathbf{x}_1, \\ \dot{x}_2 = \mathbf{B}^{-1}(\mathbf{x})[\mathbf{U}(\mathbf{x}) + \mathbf{r} + \boldsymbol{\tau}], \\ \dot{x}_1 = \mathbf{x}_2, \end{cases} \tag{7}$$

where $\mathbf{x}_1 = [q_1, q_2, \ldots, q_m]^T$, $\mathbf{x}_2 = [\dot{q}_1, \dot{q}_2, \ldots, \dot{q}_m]^T$, $\mathbf{B}(\mathbf{x}) = M(q)$, $\mathbf{U}(\mathbf{x}) = -C(q,\dot{q})\dot{q} - G(q)$, $\mathbf{r} = -f_{\mathrm{dis}}$, and $\tau = [\tau_1, \ldots, \tau_m]^T$.

We aim to design an adaptive controller that could ensure the robot manipulator system has satisfactory tracking performance under input nonlinearity and uncertain model dynamics.

The $\mathbf{B}(\mathbf{x})$ could be divided as follows:

$$\mathbf{B}(\mathbf{x}) = \mathbf{B}_d(\mathbf{x}) + \Delta_{\mathbf{B}}, \tag{8}$$

where $\mathbf{B}_d(\mathbf{x})$ component matrix is diagonal and $\Delta_{\mathbf{B}}$ component is unknown.

With (7), we could obtain

$$\begin{aligned} \mathbf{B}_d(\mathbf{x})\dot{x}_2 &= \left(I - \Delta_{\mathbf{B}}\mathbf{B}^{-1}(\mathbf{x})\right)\mathbf{U}(\mathbf{x}) + \tau \\ &\quad + \left(I - \Delta_{\mathbf{B}}\mathbf{B}^{-1}(\mathbf{x})\right)\mathbf{r} - \Delta_{\mathbf{B}}\mathbf{B}^{-1}(\mathbf{x})\tau, \\ &= \mathscr{F}(\mathbf{x}) + \mathscr{R} + \tau + p, \end{aligned} \tag{9}$$

where $\mathscr{F}(\mathbf{x}) = (I - \Delta_{\mathbf{B}}\mathbf{B}^{-1}(\mathbf{x}))\mathbf{U}(\mathbf{x}) \in R^m$, $\mathscr{R} = (I - \Delta_{\mathbf{B}}\mathbf{B}^{-1}(\mathbf{x}))\mathbf{r} \in R^m$, and $p = -\Delta_{\mathbf{B}}\mathbf{B}^{-1}(\mathbf{x})\tau \in R^m$.

The tracking errors $\mathbf{e}_i$ are represented as

$$\mathbf{s}_i = \dot{e}_i + \lambda_i \mathbf{e}_i, \tag{10}$$

$$\mathbf{e}_i = \mathbf{y}_i - \mathbf{y}_{\mathrm{di}}, \quad i = 1, \ldots, m, \tag{11}$$

where $\lambda_1, \lambda_2, \ldots, \lambda_m$ are controlled parameters.

Therefore, combining (7) with (10), we can obtain

$$\dot{s} = \mathbf{B}_d^{-1}(\mathbf{x})[\mathscr{F}(\mathbf{x}) + \mathscr{R} + \tau + p] + \mathbf{v}, \tag{12}$$

where $\mathbf{s} = [\mathbf{s}_1, \ldots, \mathbf{s}_m]^T$ and $\nu = [\nu_1, \ldots, \nu_m]^T$ with $\nu_i = -\mathbf{y}_{\mathrm{di}}^{(2)} + \lambda_i \dot{e}_i$, $i = 1, \ldots, m$.

2.5. Integral Lyapunov Analysis. An integral Lyapunov function is modeled as

$$\mathbf{V}_1 = \mathbf{s}^T \mathbf{B}_\vartheta \mathbf{s}, \tag{13}$$

where

$$\mathbf{B}_\vartheta = \int_0^1 \vartheta \mathbf{B}_\alpha \mathrm{d}\vartheta = \mathrm{diag}\left[\int_0^1 \vartheta \mathbf{B}_{\alpha ii}(\overline{x}, t\vartheta n \mathbf{s}_i q + h\mathbf{v}_i)\mathrm{d}\vartheta\right], \tag{14}$$

with $\mathbf{B}_\alpha = \mathbf{B}_d(\overline{x}, \vartheta \mathbf{s}_i + \mathbf{v}_i)\alpha = \mathrm{diag}[b_{dii}(\overline{x}, \vartheta \mathbf{s}_i + \mathbf{v}_i)\alpha_{ii}]_{m\times m}$, $\overline{x} = \mathbf{x}_1$, $\alpha \in R^{m\times m}$, and $\alpha_{11} = \cdots = \alpha_{mm}$. $\mathbf{v} = \dot{y}_d - \xi$ where $\xi = [\xi_1, \xi_2, \ldots, \xi_m]^T \in R^m$ with $\xi_i = \lambda_i \mathbf{e}_i$, $i = 1, 2, \ldots, m$.

According to (14), then (13) is remodelled as a high-dimensional Lyapunov function

$$\mathbf{V}_1 = \sum_{i=1}^{m} \mathbf{s}_i^2 \int_0^1 \vartheta \mathbf{B}_{\alpha ii}(\overline{x}, \vartheta \mathbf{s}_i + \mathbf{v}_i)\mathrm{d}\vartheta. \tag{15}$$

Based on the definition of $\mathbf{B}_\alpha$, $\mathbf{B}_\alpha$ has minimum and maximum eigenvalues $\lambda_{\min}(\mathbf{B}_\alpha)$ and $\lambda_{\max}(\mathbf{B}_\alpha)$,

$$0 \le \lambda_{\min}(\mathbf{B}_\alpha)\mathbf{s}^T\mathbf{s} \le \mathbf{s}^T\mathbf{B}_\alpha\mathbf{s} \le \lambda_{\max}(\mathbf{B}_\alpha)\mathbf{s}^T\mathbf{s}. \tag{16}$$

Considering ϑ component in $\mathbf{B}_\alpha$ function, which is independent of $\mathbf{s}$, $\overline{\mathbf{x}}$, and $\mathbf{v}$, we can obtain

$$0 \le \mathbf{s}^T\left(\int_0^1 \vartheta \mathbf{B}_\alpha \mathrm{d}\vartheta\right)\mathbf{s} \le \left(\int_0^1 \vartheta \lambda_{\max}(\mathbf{B}_\alpha)\mathrm{d}\vartheta\right)\mathbf{s}^T\mathbf{s}. \tag{17}$$

Thus, $\mathbf{V}_1 \ge 0$ is proved.

As $\mathbf{B}_\alpha$ and $\mathbf{B}_\vartheta$ are symmetric, the derivative of $\mathbf{V}_1$ is modeled as

$$\dot{V}_1 = 2\mathbf{s}^T\mathbf{B}_\vartheta\dot{s} + \mathbf{s}^T\left(\frac{\partial \mathbf{B}_\vartheta}{\partial \mathbf{s}}\dot{s}\right)\mathbf{s} + \mathbf{s}^T\left(\frac{\partial \mathbf{B}_\vartheta}{\partial \overline{x}}\dot{\overline{x}}\right)\mathbf{s} + \mathbf{s}^T\left(\frac{\partial \mathbf{B}_\vartheta}{\partial \mathbf{v}}\dot{\nu}\right)\mathbf{s}, \tag{18}$$

with

$$\begin{aligned}
\frac{\partial \mathbf{B}_\vartheta}{\partial \mathbf{s}}\dot{s} &= \mathrm{diag}\left[\int_0^1 \vartheta \frac{\partial \mathbf{B}_{\alpha ii}}{\partial \mathbf{s}_i}\dot{s}_i \mathrm{d}\vartheta\right], \\
\frac{\partial \mathbf{B}_\vartheta}{\partial \overline{x}}\dot{\overline{x}} &= \mathrm{diag}\left[\int_0^1 \vartheta \sum_{j=1}^{m} \frac{\partial \mathbf{B}_{\alpha ii}}{\partial \overline{x}_j}\dot{\overline{x}}_j \mathrm{d}\vartheta\right], \\
\frac{\partial \mathbf{B}_\vartheta}{\partial \mathbf{v}}\dot{\nu} &= \mathrm{diag}\left[\int_0^1 \vartheta \frac{\partial \mathbf{B}_{\alpha ii}}{\partial \mathbf{v}_i}\dot{\nu}_i \mathrm{d}\vartheta\right], \quad i = 1, \ldots, m.
\end{aligned} \tag{19}$$

Considering the following equations,

$$\frac{\partial \mathbf{B}_\vartheta}{\partial \mathbf{s}}\mathbf{s} = \mathrm{diag}\left[\int_0^1 \vartheta \frac{\partial \mathbf{B}_{\alpha ii}}{\partial \mathbf{s}_i}\mathbf{s}_i \mathrm{d}\vartheta\right] = \int_0^1 \vartheta^2 \frac{\partial \mathbf{B}_\alpha}{\partial \vartheta}\mathrm{d}\vartheta, \tag{20}$$

we have

$$\begin{aligned}
\mathbf{s}^T\left(\frac{\partial \mathbf{B}_\vartheta}{\partial \mathbf{s}}\dot{s}\right)\mathbf{s} &= \mathbf{s}^T\left(\left[\vartheta^2\mathbf{B}_\alpha\right]_0^1 - 2\int_0^1 \vartheta \mathbf{B}_\alpha \mathrm{d}\vartheta\right)\dot{s} \\
&= \mathbf{s}^T\mathbf{B}_\alpha\dot{s} - 2\mathbf{s}^T\mathbf{B}_\vartheta\dot{s}.
\end{aligned} \tag{21}$$

As ϑ is a scalar, and $\sigma = \vartheta \mathbf{s}_i$, we have $(\partial \mathbf{B}_\vartheta/\partial \mathbf{v})\mathbf{s} = \mathrm{diag}\left[\int_0^1 \vartheta(\partial \mathbf{B}_{\alpha ii}/\partial \mathbf{v}_i)\mathbf{s}_i \mathrm{d}\vartheta\right] = \int_0^1 \vartheta(\partial \mathbf{B}_\alpha/\partial\vartheta)\mathrm{d}\vartheta$ and $\nu = -\dot{\nu}$. Then, we have

$$\begin{aligned}
\mathbf{s}^T\left(\frac{\partial \mathbf{B}_\vartheta}{\partial \mathbf{v}}\dot{\nu}\right)\mathbf{s} &= \mathbf{s}^T\left(-\int_0^1 \vartheta \frac{\partial \mathbf{B}_\alpha}{\partial \vartheta}\mathrm{d}\vartheta\right)\mathbf{v} \\
&= -\mathbf{s}^T\mathbf{B}_\alpha\mathbf{v} + \mathbf{s}^T\int_0^1 \mathbf{B}_\alpha \mathbf{v}\,\mathrm{d}\vartheta.
\end{aligned} \tag{22}$$

Combining (21) and (22), (18) can be rewritten as

$$\dot{V}_1 = \mathbf{s}^T\mathbf{B}_\alpha\dot{s} - \mathbf{s}^T\mathbf{B}_\alpha + \mathbf{s}^T\left[\left(\frac{\partial \mathbf{B}_\vartheta}{\partial \overline{x}}\dot{\overline{x}}\right)\mathbf{s} + \int_0^1 \mathbf{B}_\alpha \mathbf{v}\mathrm{d}\vartheta\right]. \tag{23}$$

Considering (12), we rewritten (23) as

$$\begin{aligned}
\dot{V}_1 &= \mathbf{s}^T\mathbf{B}_\alpha\mathbf{B}_d^{-1}(\mathbf{x})[\mathscr{F}(\mathbf{x}) + \tau + \mathscr{R} + p] \\
&\quad + \mathbf{s}^T\left[\left(\frac{\partial \mathbf{B}_\vartheta}{\partial \overline{x}}\dot{\overline{x}}\right)\mathbf{s} + \int_0^1 \mathbf{B}_\alpha \mathbf{v}\mathrm{d}\vartheta\right].
\end{aligned} \tag{24}$$

Since $\mathbf{B}_d$, α, and $\mathbf{B}_d\alpha$ are symmetric, we have

$$\mathbf{B}_\alpha\mathbf{B}_d^{-1}(\mathbf{x}) = \mathbf{B}_d(\mathbf{x})\alpha\mathbf{B}_d^{-1}(\mathbf{x}) = \alpha, \tag{25}$$

and rewrite (24) as

$$\dot{V}_1 = \mathbf{s}^T\alpha[\mathscr{F}(\mathbf{x}) + \tau + \mathscr{R} + p] + \mathbf{s}^T\left[\left(\frac{\partial \mathbf{B}_\vartheta}{\partial \overline{x}}\dot{\overline{x}}\right)\mathbf{s} + \int_0^1 \mathbf{B}_\alpha \mathbf{v}\mathrm{d}\vartheta\right]. \tag{26}$$

Considering (14) and $\mathbf{B}_\alpha = \mathbf{B}_d\alpha$,

$$\begin{aligned}
\dot{V}_1 &= \mathbf{s}^T\alpha[\mathscr{F}(\mathbf{x}) + \tau + \mathscr{R} + p] \\
&\quad + \mathbf{s}^T\left[\int_0^1 \vartheta\left(\frac{\partial \mathbf{B}_\alpha}{\partial \overline{x}}\dot{\overline{x}}\right)\mathbf{s}\mathrm{d}\vartheta + \int_0^1 \mathbf{B}_\alpha \mathbf{v}\mathrm{d}\vartheta\right] \\
&= \mathbf{s}^T\alpha[\mathscr{F}(\mathbf{x}) + \Phi + \tau + \mathscr{R} + p].
\end{aligned} \tag{27}$$

where

$$\begin{aligned}
\Phi &= \int_0^1 \vartheta\left(\frac{\partial \mathbf{B}_d}{\partial \overline{x}}\dot{\overline{x}}\right)\mathbf{s}\mathrm{d}\vartheta + \int_0^1 \mathbf{B}_d \nu \mathrm{d}\vartheta, \\
\frac{\partial \mathbf{B}_d}{\partial \overline{x}}\dot{\overline{x}} &= \mathrm{diag}\left[\sum_{j=1}^{m} \frac{\partial b_{dii}}{\partial \overline{x}_j}\dot{\overline{x}}_j\right], \quad i = 1, \ldots, m.
\end{aligned} \tag{28}$$

2.6. Disturbance-Observer-Based Fuzzy Controller. As the accurate and complete dynamics of a robot manipulator is difficult to obtain, especially in complex environments with unknown external disturbance, a fuzzy logic system is adopted for the estimation of unknown functions in the robot manipulator. Generally, the fuzzy rules are given as

$$\Lambda_i: \text{ if } Z_1 \text{ is } K_1^i \text{ and }, \ldots, \text{ and } Z_l \text{ is } K_l^i, \text{ then } h \text{ is } h_i, \tag{29}$$

where h_i represents i_{th} fuzzy rule.

$$h(Z) = \frac{\sum_{l=1}^{m} h^l\left(\prod_{j=1}^{n} \varphi\left(Z_j\right)\right)}{\sum_{l=1}^{m}\left(\prod_{j=1}^{n} \varphi\left(Z_j\right)\right)} = \Theta^T S(Z), \tag{30}$$

where $Z = [Z_1, Z_2, \ldots, Z_n] \in R^n$ is the input variable; $S_i = ((\prod_{j=1}^{n} \varphi(Z_j))/(\sum_{l=1}^{m}(\prod_{j=1}^{n} \varphi(Z_j))))$ are the fuzzy basis functions; m is the number of fuzzy rules; and W denotes the adaptable weight parameters.

In this study, the uncertain term $\mathscr{F}(\mathbf{x})$ is estimated as

$$\mathscr{F}(\mathbf{x}) = -\Theta^{*T} S(Z) - \varsigma, \tag{31}$$

where $Z = [\mathbf{x}_1^T, \mathbf{x}_2^T]^T$ and ς represents the approximate error and $\|\varsigma\| \le \varsigma^*$ $(\varsigma^* > 0)$.

Then, we rewritten (9) as

$$\mathbf{B}_d(\mathbf{x})\dot{x}_2 = -\Theta^{*T} S(Z) - \varsigma + \mathscr{R} + \tau + p. \tag{32}$$

To eliminate the effect of the external disturbance and unknown terms in the system, a disturbance observer is utilized in the controller design. We define $D = \mathscr{R} + p - \varsigma$, and (32) can be represented as

$$\mathbf{B}_d(\mathbf{x})\dot{x}_2 = -\Theta^{*T} S(Z) + \tau + D. \tag{33}$$

As in the robotic system, the actuator and input saturation exist [29]; the motor torque is normally assumed to be constrained with saturation in practical. Therefore, $p = -\Delta_{\mathbf{B}}\mathbf{B}^{-1}(\mathbf{x})\tau$ is bounded. In this study, the $\mathbf{r}$ in this robot manipulator system is assumed as bounded with $\|\mathbf{r}\| \le d_c$, where d_c is a positive constant. As the derivative of a differential continuous function with bounded constraints is also bounded [30], we can obtain $\|\dot{D}\| \le \varrho$, where $\varrho > 0$.

For the disturbance observer design, an auxiliary variable Ω is defined as $\Omega = D - \Psi\mathbf{x}_2$ with $\Psi = \Psi^T > 0$. With (33), we can obtain

$$\begin{aligned}\dot{\Omega} &= \dot{D} - \Psi\dot{\mathbf{x}}_2 \\ &= \dot{D} - \Psi\mathbf{B}_d^{-1}(\mathbf{x})\left[-\Theta^{*T} S(Z) + \tau + D\right].\end{aligned} \tag{34}$$

Then, the estimate of $\dot{\Omega}$ is calculated as

$$\dot{\widehat{\Omega}} = -\Psi\mathbf{B}_d^{-1}(\mathbf{x})\left[\tau + \widehat{D} - \widehat{\Theta}^T S(Z)\right], \tag{35}$$

where $\widehat{D} = \widehat{\Omega} + \Psi\mathbf{x}_2$ and is the estimate of D. Then, we define $\widetilde{D} = D - \widehat{D}$ as the disturbance estimate error, and we have

$$\widetilde{\Omega} = \Omega - \widehat{\Omega} = D - \widehat{D} = \widetilde{D}. \tag{36}$$

Then, the derivative of $\widetilde{D}$ is computed as

$$\begin{aligned}\dot{\widetilde{D}} &= \dot{\widetilde{\Omega}} = \dot{\Omega} - \dot{\widehat{\Omega}} \\ &= \dot{D} - \Psi\mathbf{B}_d^{-1}(\mathbf{x})\left[\widetilde{D} + \widetilde{\Theta}^T S(Z)\right],\end{aligned} \tag{37}$$

with $\widetilde{\Theta} = \widehat{\Theta} - \Theta^*$.

Based on the disturbance observer [31] and fuzzy logic rules, the control law of this robot manipulator is developed as

$$\tau = \widehat{\Theta}^T S(Z) - \Phi - K_1\alpha\mathbf{s} - \widehat{D}. \tag{38}$$

The updated law of the fuzzy controller is developed as

$$\dot{\widehat{\Theta}}_i = -\Gamma_i\left[S_i(Z)\alpha_{ii}\mathbf{s}_i + \varepsilon\widehat{\Theta}_i\right], \tag{39}$$

where Γ_i and ε are positive constants.

Theorem 1. *According to the designed controller in (38) and the disturbance-observer-based fuzzy controller, all closed-loop signals are uniformly bounded in this complex environment with unknown disturbances and model uncertainties (proof is shown in Appendix A).*

3. Simulation

The EMG-driven NMS model was implemented in OpenSim 3.3 through the calibrated EMG-informed NMS modelling toolbox (CEINMS) [21]. OpenSim was also used to calculate musculotendon lengths and moment arms using joint angles through the scaled musculoskeletal model [32]. CEINMS was then employed to calibrate a subject-specific EMG-driven NMS model to predict joint torques. A generic reaching task was simulated with a musculoskeletal arm model (Figure 2), and the data were acquired from a publicly available database (https://simtk.org/frs/index.php?group_id=657) [33]. The input data include EMG signals and joint kinematics of right arm shoulder and elbow. The EMG signals of 6 muscles of the right arm were simulated through static optimization tool (resolving the net joint moments into individual muscle forces by minimizing the sum of squared muscle activations) in OpenSim, including triceps long, triceps lateral, triceps medial, biceps long, biceps short, and brachialis.

Before using the EMG-driven NMS model to predict joint torque, a calibration process was applied to obtain a subject-specific EMG-driven NMS model with individual's muscle-tendon properties. To perform the calibration, inverse dynamics was used to calculate the joint moment as measured joint moments. Inverse dynamics calculated the forces and torques of joints by solving dynamic equation of motion of the user as shown in the following equation:

$$M(q)\ddot{q} + C(q, \dot{q}) + G(q) = \tau, \tag{40}$$

where $q, \dot{q}, \ddot{q}$ are the position, velocity, and acceleration of the generalised coordinates; $M(q)$ is the mass matrix; $C(q, \dot{q})$ is the centripetal and Coriolis forces matrix; $G(q)$ is the gravitational forces matrix; and τ is the vector of unknown generalised forces.

Figure 2: The reaching task illustration of the manipulator.

During the calibration of the subject-specific EMG-driven NMS model, optimal fibre length l_0^m and tendon slack length l_s^t of each MTU were bounded within ±15% from their initial values, and muscle activation dynamics parameters A, C_1, C_2 were calibrated globally. The shape factor A was bounded between −3 and 0 and coefficients C_1, C_2 were bounded between −1 and 1. A strength coefficient constrained between 0.5 and 2.5 was assigned to each MTU and was used to calibrate maximum isometric force. During the calibration, these subject-specific parameters were refined by an optimization algorithm to minimize the error between estimated and measured/actual ankle joint torques [21].

Correlation analysis of joint torque estimated via inverse dynamics and EMG-driven NMS model was carried out across all trials using MATLAB (MatlabR2018a, MathWorks Inc., Natick, MA, USA). A significance level of 0.05 was set for all statistical tests.

For the robot manipulator, our aim was to design a controller that could complete tasks with human-like characteristics as to follow the desired velocity. In the system, we consider 2-DOFs shoulder and elbow manipulator, and the dynamic modelling of the shoulder and elbow manipulator is modeled as

$$M(q)\ddot{q} + C(q,\dot{q})\dot{q} + G(q) + f_{\text{dis}} = \tau, \tag{41}$$

where τ is the joint torque and $q = [q_1, q_2]^T$. We model $M(q)$, $C(q,\dot{q})$, $G(q)$, and f_{dis} as

$$\begin{aligned} M(q) &= \begin{bmatrix} M_{11} & M_{12} \\ M_{21} & M_{22} \end{bmatrix}, \\ C(q,\dot{q}) &= \begin{bmatrix} C_{11} & C_{12} \\ C_{21} & C_{22} \end{bmatrix}, \\ G(q) &= \begin{bmatrix} G_1 \\ G_2 \end{bmatrix}, \\ f_{\text{dis}} &= \begin{bmatrix} D_1 \\ D_2 \end{bmatrix}, \end{aligned} \tag{42}$$

where $M_{11} = m_1 l_{c1}^2 + m_2(l_1^2 + l_{c2}^2 + 2l_1 l_{c2}\cos q_2) + I_1 + I_2$, $M_{12} = m_2(l_{c2}^2 + l_1 l_{c2}\cos q_2) + I_2$, $M_{21} = m_2(l_{c2}^2 + l_1 l_{c2}\cos q_2) + I_2$, $M_{22} = m_2 l_{c2}^2 + I_2$; $C_{11} = -m_2 l_1 l_{c2}\dot{q}_2 \sin q_2$, $C_{12} = -m_2 l_1 l_{c2}(\dot{q}_1 + \dot{q}_2)\sin q_2$, $C_{21} = m_2 l_1 l_{c2}\dot{q}_1 \sin q_2$, $C_{22} = 0$; $G_1 = (m_1 l_{c2} + m_2 l_1)\, g\cos q_1 + m_2 l_{c2} g\cos(q_1 + q_2)$, $G_2 = m_2 l_{c2} g\cos(q_1 + q_2)$; $D_1 = 0.21\cos q_2^2 + 0.04\sin(0.3 q_2 t)$; and $D_1 = 0.12\sin q_1^2 + 0.03\sin(0.2 q_1 t)$.

The robotic system parameters are modeled as $m_1 = 2$ kg, $m_2 = 1.5$ kg, $l_1 = 0.35$ m, $l_2 = 0.2$ m, $g = 9.81$ m/s^2, $I_1 = (1/4)m_1 l_1^2$, and $I_2 = (1/2)m_2 l_2^2$, and l_c is the center of mass with $l_c = (l/2)$.

We transform (41) into the model we used in (7), which is

$$\begin{cases} \mathbf{y} = \mathbf{x}_1, \\ \dot{x}_2 = \mathbf{B}^{-1}(\mathbf{x})[\mathbf{U}(\mathbf{x}) + \mathbf{r} + \boldsymbol{\tau}], \\ \dot{x}_1 = \mathbf{x}_2, \end{cases} \tag{43}$$

where $x_1 = [q_1, q_2]^T$, $x_2 = [\dot{q}_1, \dot{q}_2]^T$, $\mathbf{B}(x) = M(q)$, $\mathbf{U}(\mathbf{x}) = -C(q,\dot{q})\dot{q}_2 - G(q)$, $\mathbf{r} = -f_{\text{dis}}$, and τ is the joint torque.

Let $\widehat{\theta}_i(0) = [0, \ldots, 0]^T$ be the initial values of the adaptive law (39). The design parameters' values were set to $\alpha = I_{2\times 2}$, $B_d(x) = \text{diag}[\cos x_1(2) + 2, 1 + 0.5\sin x_1(1)]$, $\lambda_{11} = \lambda_{21} = 24$, $\Gamma_1 = \Gamma_2 = \Gamma_{\tau 1} = \Gamma_{\tau 2} = 1$, and $\sigma = \sigma_\tau = 9$.

The joint torque (normalized by the arm mass) estimated via inverse dynamics and EMG-driven NMS model is shown in Figures 3 and 4. The results of the correlation analysis showed that there was a significant correlation of joint torque estimated via inverse dynamics and EMG-driven NMS model ($p < 0.01$). The Pearson coefficients $r_1 = 0.991$ and $r_2 = 0.507$ were observed at the shoulder and elbow flexion/extension DOFs in the arm reaching movement, respectively. The root mean square error (RMSE) of shoulder flexion/extension torque between inverse dynamics and EMG-driven NMS model was 0.048 Nm/kg. Similar RMSE 0.046 Nm/kg was observed at the elbow flexion/extension DOFs in the arm reaching movement. Figures 5 and 6 demonstrated the desired and actual joint angular velocity of the robot manipulator in the reaching task, and the results validated the effectiveness of the proposed controller which could complete the task with users-like adaptivity and had a good performance.

4. Discussion

We developed a disturbance-observer-based fuzzy control framework that fully incorporates a robot manipulator system with an EMG-driven NMS model and could be applied in the controlling of the movement of robot manipulators with human-like characteristics. In the developed framework, a reaching task for a robot manipulator was studied to test performance of the disturbance-observer-based fuzzy controller. We found that the user's intention was well-predicted by the EMG-driven NMS model and then transmitted to the desired velocities of the robot manipulator system, which allows the robot manipulator system behave with human-like adaptivity. In the robot manipulator system with external disturbances and model uncertainties, the proposed disturbance-observer-based fuzzy control was also able to provide a good performance of motion tracking. In the current paper, the control framework we proposed in general is useful for obtaining the human-like characteristics, as well as simulating the control strategy in the robot manipulator system, and thus be of

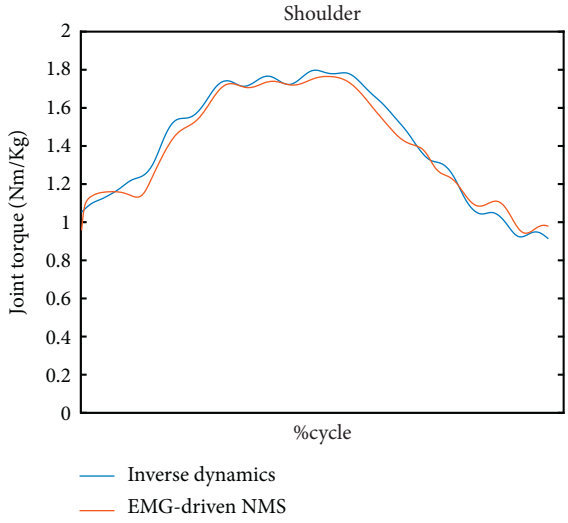

Figure 3: Shoulder joint torque (normalized by body mass) estimated via inverse dynamics and EMG-driven NMS model.

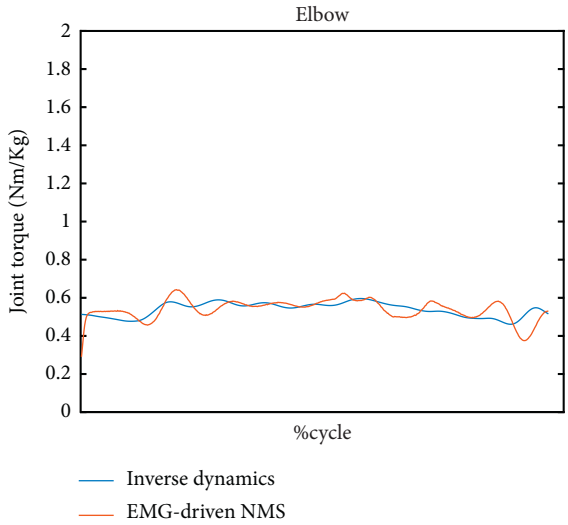

Figure 4: Elbow joint torque (normalized by body mass) estimated via inverse dynamics and EMG-driven NMS model.

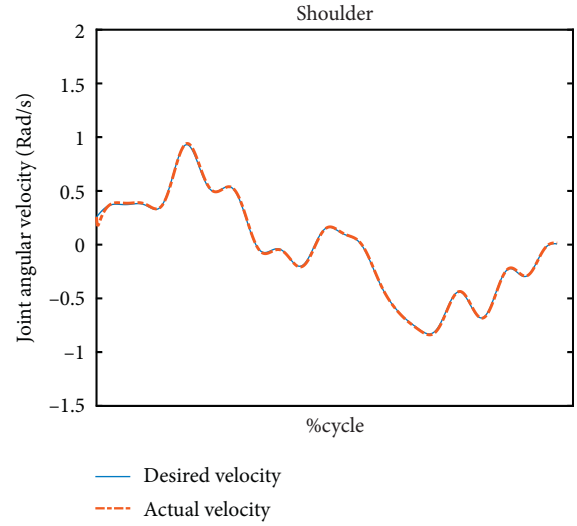

Figure 5: The desired and actual angular velocity of the shoulder.

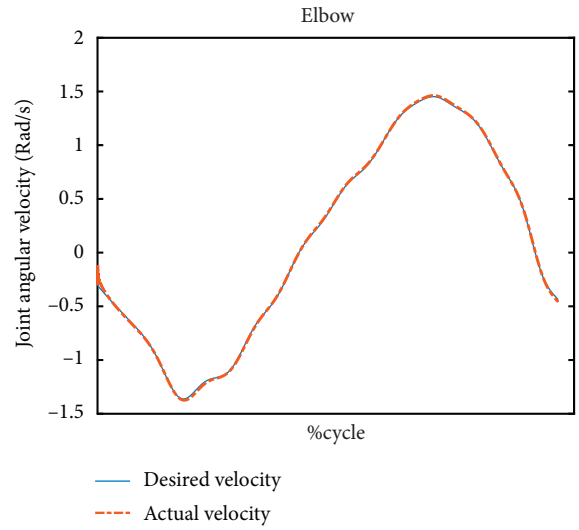

Figure 6: The desired and actual angular velocity of the elbow.

large benefit for teleoperation robot manipulator applications.

EMG-driven NMS model is a popular method in users' motion intention (joint torque) estimation [34–36]. The EMG-driven NMS model uses mathematical equations to reproduce the transformations from EMG signal generation and joint angles to musculotendon forces and joint torques. To better predict joint torque, subject-specified EMG-driven model was calibrated with personalized musculoskeletal geometry such as moment arms and muscle characteristics. During the calibration, these subject-specific parameters were refined by an optimization algorithm to minimize the error between estimated and measured/actual ankle joint torques. With the mathematical equations approximately reproducing the transformations and optimization algorithm included in the calibration process, inevitable error existed in the EMG-driven NMS model when mapping EMG signals and angles into the joint torque. Despite this, the EMG-driven NMS model was able to estimate joint torque in close agreement to the reference data (with RMSE lower than 0.048 Nm/kg).

It is important to notice that unknown dynamics and external disturbance commonly exist in robotic manipulator systems. Fuzzy logic system [37], neural network [38], and disturbance observer [39] are commonly applied to solve these problems and maintain the system stability. Su et al. [40] integrated a fuzzy compensator into a teleoperation controller for a robot manipulator, and this controller was able to guarantee a safety-enhanced behavior in the null space. Li et al. [41] utilized a disturbance observer to compensate for the external disturbance in an admittance control for an upper robotic exoskeleton and guaranteed the robustness of the robotic arm. In the current study, a disturbance-observer-based controller with a high-dimensional integral-type Lyapunov function was developed for a robotic

manipulator with external disturbances and model uncertainties. The good tracking performance (Figures 5 and 6) demonstrate the effectiveness of the proposed control framework and the semiglobally uniformly ultimate boundness of the closed-loop control system is also established.

One limitation of this study was that only reaching task at one speed was studied as an example in the proposed framework. Reaching task at different speeds as well as different situations and other daily activities such as grasp could be also tested in the proposed framework. Another limitation was that we only tested the control framework in a simulation environment with one subject data. Large sample size of subjects could be enrolled in the future study to see whether the proposed control framework would be able to generalize across subjects.

5. Conclusions

We developed an adaptive control framework that fully incorporates a robot manipulator system with an EMG-driven NMS model and use it to control the motion of the robot manipulator with human-like characteristics. In the developed framework, an example was studied to test performance of the disturbance-observer-based fuzzy controller, which was applied to a robot manipulator during a reaching task. We found that the EMG-driven NMS model was able to predict the user's intention (desired torque) and transmitted these human-like characteristics to the desired trajectories of the robot manipulator system. Moreover, external disturbances as well as model uncertainties were simulated in the robot manipulator system, and the proposed adaptive fuzzy controller integrated with a disturbance observer was able to provide a good performance of motion tracking. In the current paper, the control framework we proposed in general is useful for obtaining the human-like characteristics, as well as simulating the control strategy in the robot manipulator system that is subjected to realistic conditions, such as model uncertainties and external disturbances, and thus be of large benefit for teleoperation robot manipulator applications.

Appendix

Proof of the Proposed Lyapunov Function Stability

The Lyapunov function candidate is modeled as

$$\mathbf{V}_2 = \mathbf{V}_1 + \frac{1}{2}\widetilde{D}^T\widetilde{D} + \frac{1}{2}\sum_{i=1}^{m}\widetilde{\Theta}_i^T\Gamma_i^{-1}\widetilde{\Theta}_i. \tag{A.1}$$

Based on (31), the derivative of $\mathbf{V}_2$ is calculated as

$$\dot{V}_2 = \mathbf{s}^T\alpha\left[-\Theta^{*T}S(Z) - \varsigma + \Phi + \tau + \mathscr{R} + p\right] + \widetilde{D}^T\dot{\widetilde{D}} + \sum_{i=1}^{m}\widetilde{\Theta}_i^T\Gamma_i^{-1}\dot{\widetilde{\Theta}}_i. \tag{A.2}$$

Considering (33), (38), and $D = \mathscr{R} + p - \varsigma$, we have

$$\dot{V}_2 = \mathbf{s}^T\alpha\left[\widetilde{\Theta}S(Z) + \widetilde{D} - K_1\alpha s\right] + \widetilde{D}^T\dot{\widetilde{D}} + \sum_{i=1}^{m}\widetilde{\Theta}_i^T\Gamma_i^{-1}\dot{\widetilde{\Theta}}_i. \tag{A.3}$$

Considering $\|\dot{D}\|$ is bounded, $\|S(Z)\| \le \delta$, (37), (39), and the following terms

$$\mathbf{s}^T\alpha\widetilde{D} \le \frac{\mathbf{s}^T\alpha\alpha\mathbf{s}}{2} + \frac{\widetilde{D}^T\widetilde{D}}{2},$$
$$\widetilde{D}^T\dot{D} \le \frac{\widetilde{D}^T\widetilde{D}}{2} + \frac{\|\dot{D}\|^2}{2}, \tag{A.4}$$
$$\sum_{i=1}^{m}\widetilde{\Theta}_i^T S_i(Z)\mathbf{s}_i\alpha_{ii} = \mathbf{s}^T\alpha\widetilde{\Theta}^T S(Z),$$

we have

$$\dot{V}_2 \le -\mathbf{s}^T\alpha\left(K_1 - 0.5I_{m\times m}\right)\alpha\mathbf{s} + \frac{\varrho^2}{2} - \widetilde{D}^T\left(\Psi\mathbf{B}_d^{-1} - 2I_{m\times m}\right)\widetilde{D} + \frac{\varepsilon\left\|\Theta^*\right\|^2}{2}, \tag{A.5}$$
$$-\frac{\varepsilon - \Psi\mathbf{B}_d^{-1}\delta}{2}\sum_{j=1}^{m}\widetilde{\Theta}_i^T\widetilde{\Theta}_i$$

where $\widetilde{D}^T\Psi\mathbf{B}_d^{-1}\widetilde{\Theta}^T S(Z) \le (\|\widetilde{D}\|^2)/2 + (\|\Psi\mathbf{B}_d^{-1}S(Z)\|\widetilde{\Theta}\|^2)/2)$ and $-\varepsilon\widetilde{\Theta}_i^T\widehat{\Theta}_i = -\varepsilon\|\widetilde{\Theta}_i\|^2 - \varepsilon\widetilde{\Theta}_i^T\Theta_i^* \le -((\varepsilon\|\widetilde{\Theta}_i\|^2)/2) + ((\varepsilon\|\Theta_i^*\|^2)/2)$.

If we choose K_1, Ψ, and ε appropriately satisfying $\lambda_{\min}(\alpha(K_1 - 0.5I_{m\times m})\alpha) \ge \int_0^1 \vartheta\lambda_{\max}(\mathbf{B}_\alpha)\mathrm{d}\vartheta$, $\Psi\mathbf{B}_d^{-1} - 2I_{m\times m} > 0$, and $\varepsilon - \Psi\mathbf{B}_d^{-1}\delta > 0$, we can obtain

$$\dot{V}_2 \le -\kappa\mathbf{V}_2 + C, \tag{A.6}$$

where

$$\kappa = \min\left(\begin{array}{c}\lambda_{\min}\left(\Psi\mathbf{B}_d^{-1} - 2I_{m\times m}\right) \\ \dfrac{\varepsilon - \Psi\mathbf{B}_d^{-1}\delta}{\lambda_{\max}\left(\sum_{i=1}^{m}\Gamma_i^{-1}\right)}, \quad 1\end{array}\right), \tag{A.7}$$
$$C = \frac{\varepsilon\left\|\Theta^*\right\|^2}{2} + \frac{\varrho^2}{2}.$$

By multiplying $e^{\kappa t}$ and integrating the both sides of inequality (A.6), we have

$$\mathbf{V}_2 \le \left(\mathbf{V}_2(0) - \frac{C}{\kappa}\right)e^{-\kappa t} + \frac{C}{\kappa} \le \mathbf{V}_2(0) + \frac{C}{\kappa}. \tag{A.8}$$

Based on (A.8), $\mathbf{V}_2$ is ultimately bounded as $t \longrightarrow \infty$; $\widetilde{D}$, $\mathbf{s}$, and $\widetilde{\Theta}$ are also bounded.

Data Availability

The data supporting this study is from a previously reported study, which has been cited at relevant place within the text as reference [33]. The dataset are available at (https://simtk.org/frs/index.php?group_id=657).

Conflicts of Interest

The authors declare that the research was conducted in the absence of any commercial or financial relationships that could be construed as a potential conflicts of interest.

References

[1] H. Su, Y. Hu, H. R. Karimi, A. Knoll, G. Ferrigno, and E. De Momi, "Improved recurrent neural network-based manipulator control with remote center of motion constraints: experimental results," *Neural Networks*, vol. 131, pp. 291–299, 2020.

[2] C. Yang, G. Peng, Y. Li, R. Cui, L. Cheng, and Z. Li, "Neural networks enhanced adaptive admittance control of optimized robot–environment interaction," *IEEE Transactions on Cybernetics*, vol. 49, no. 7, pp. 2568–2579, 2018.

[3] P. K. Artemiadis and K. J. Kyriakopoulos, "Teleoperation of a robot manipulator using EMG signals and a position tracker," in *Proceedings of the 2005 IEEE/RSJ International Conference on Intelligent Robots and Systems*, pp. 1003–1008, IEEE, Edmonton, Canada, August 2005.

[4] H. Huang, T. Zhang, C. Yang, and C. P. Chen, "Motor learning and generalization using broad learning adaptive neural control," *IEEE Transactions on Industrial Electronics*, vol. 67, no. 10, pp. 8608–8617, 2019.

[5] W. Qi, H. Su, and A. Aliverti, "A smartphone-based adaptive recognition and real-time monitoring system for human activities," *IEEE Transactions on Human-Machine Systems*, vol. 50, no. 5, pp. 414–423, 2020.

[6] Z. Li, Y. Yuan, L. Luo et al., "Hybrid brain/muscle signals powered wearable walking exoskeleton enhancing motor ability in climbing stairs activity," *IEEE Transactions on Medical Robotics and Bionics*, vol. 1, no. 4, pp. 218–227, 2019.

[7] W. Ryu, B. Han, and J. Kim, "Continuous position control of 1 dof manipulator using EMG signals," in *Proceedings of the 2008 Third International Conference on Convergence and Hybrid Information Technology*, vol. 1, pp. 870–874, IEEE, Busan, South Korea, November 2008.

[8] N. Bu, M. Okamoto, and T. Tsuji, "A hybrid motion classification approach for EMG-based human–robot interfaces using Bayesian and neural networks," *IEEE Transactions on Robotics*, vol. 25, no. 3, pp. 502–511, 2009.

[9] C. Yang, J. Luo, C. Liu, M. Li, and S.-L. Dai, "Haptics electromyography perception and learning enhanced intelligence for teleoperated robot," *IEEE Transactions on Automation Science and Engineering*, vol. 16, no. 4, pp. 1512–1521, 2019.

[10] Y. Hu, X. Wu, P. Geng, and Z. Li, "Evolution strategies learning with variable impedance control for grasping under uncertainty," *IEEE Transactions on Industrial Electronics*, vol. 66, no. 10, pp. 7788–7799, 2018.

[11] K. Yi, J. Han, X. Liang, and Y. He, "Contact transition control with acceleration feedback enhancement for a quadrotor," *ISA Transactions*, 2020.

[12] G. Chen, H. Cao, J. Conradt, H. Tang, F. Rohrbein, and A. Knoll, "Event-based neuromorphic vision for autonomous driving: a paradigm shift for bio-inspired visual sensing and perception," *IEEE Signal Processing Magazine*, vol. 37, no. 4, pp. 34–49, 2020.

[13] C. Yang, Y. Jiang, J. Na, Z. Li, L. Cheng, and C.-Y. Su, "Finite-time convergence adaptive fuzzy control for dual-arm robot with unknown kinematics and dynamics," *IEEE Transactions on Fuzzy Systems*, vol. 27, no. 3, pp. 574–588, 2019.

[14] H. Su, W. Qi, C. Yang, J. Sandoval, G. Ferrigno, and E. D. Momi, "Deep neural network approach in robot tool dynamics identification for bilateral teleoperation," *IEEE Robotics and Automation Letters*, vol. 5, no. 2, pp. 2943–2949, 2020.

[15] H. Lin, T. Zhang, Z. Chen, H. Song, and C. Yang, "Adaptive fuzzy Gaussian mixture models for shape approximation in robot grasping," *International Journal of Fuzzy Systems*, vol. 21, no. 4, pp. 1026–1037, 2019.

[16] W. He, Y. Sun, Z. Yan, C. Yang, Z. Li, and O. Kaynak, "Disturbance observer-based neural network control of cooperative multiple manipulators with input saturation," *IEEE Transactions on Neural Networks and Learning Systems*, vol. 31, no. 5, pp. 1735–1746, 2019.

[17] R. Yang, C. Yang, M. Chen, and J. Na, "Adaptive impedance control of robot manipulators based on Q-learning and disturbance observer," *Systems Science & Control Engineering*, vol. 5, no. 1, pp. 287–300, 2017.

[18] S. Qiu, Z. Li, W. He, L. Zhang, C. Yang, and C.-Y. Su, "Brain–machine interface and visual compressive sensing-based teleoperation control of an exoskeleton robot," *IEEE Transactions on Fuzzy Systems*, vol. 25, no. 1, pp. 58–69, 2016.

[19] H. Su, C. Yang, G. Ferrigno, and E. De Momi, "Improved human-robot collaborative control of redundant robot for teleoperated minimally invasive surgery," *IEEE Robotics and Automation Letters*, vol. 4, no. 2, pp. 1447–1453, 2019.

[20] H. Su, W. Qi, Y. Hu, H. R. Karimi, G. Ferrigno, and E. De Momi, "An incremental learning framework for human-like redundancy optimization of anthropomorphic manipulators," *IEEE Transactions on Industrial Informatics*, 2021.

[21] C. Pizzolato, D. G. Lloyd, M. Sartori et al., "CEINMS: a toolbox to investigate the influence of different neural control solutions on the prediction of muscle excitation and joint moments during dynamic motor tasks," *Journal of Biomechanics*, vol. 48, no. 14, pp. 3929–3936, 2015.

[22] M. Sartori, M. Reggiani, D. G. Lloyd, and E. Pagello, "A neuromusculoskeletal model of the human lower limb: towards EMG-driven actuation of multiple joints in powered orthoses," in *Proceedings of the 2011 IEEE International Conference on Rehabilitation Robotics*, pp. 1–6, IEEE, Zurich, Switzerland, July 2011.

[23] D. G. Lloyd and T. F. Besier, "An EMG-driven musculoskeletal model to estimate muscle forces and knee joint moments in vivo," *Journal of Biomechanics*, vol. 36, no. 6, pp. 765–776, 2003.

[24] T. S. Buchanan, D. G. Lloyd, K. Manal, and T. F. Besier, "Neuromusculoskeletal modeling: estimation of muscle forces and joint moments and movements from measurements of neural command," *Journal of Applied Biomechanics*, vol. 20, no. 4, pp. 367–395, 2004.

[25] H. X. Hoang, C. Pizzolato, L. E. Diamond, and D. G. Lloyd, "Subject-specific calibration of neuromuscular parameters enables neuromusculoskeletal models to estimate physiologically plausible hip joint contact forces in healthy adults," *Journal of Biomechanics*, vol. 80, pp. 111–120, 2018.

[26] N. Lotti, M. Xiloyannis, G. Durandau et al., "Adaptive model-based myoelectric control for a soft wearable arm exosuit: a new generation of wearable robot control," *IEEE Robotics & Automation Magazine*, vol. 27, no. 1, pp. 43–53, 2020.

[27] Q. Wu, X. Wang, B. Chen, and H. Wu, "Patient-active control of a powered exoskeleton targeting upper limb rehabilitation training," *Frontiers in Neurology*, vol. 9, p. 817, 2018.

[28] Z. Li, Z. Huang, W. He, and C.-Y. Su, "Adaptive impedance control for an upper limb robotic exoskeleton using biological signals," *IEEE Transactions on Industrial Electronics*, vol. 64, no. 2, pp. 1664–1674, 2016.

[29] W. Sun, Z. Zhao, and H. Gao, "Saturated adaptive robust control for active suspension systems," *IEEE Transactions on Industrial Electronics*, vol. 60, no. 9, pp. 3889–3896, 2012.

[30] L. Zhang, Z. Li, and C. Yang, "Adaptive neural network based variable stiffness control of uncertain robotic systems using disturbance observer," *IEEE Transactions on Industrial Electronics*, vol. 64, no. 3, pp. 2236–2245, 2016.

[31] D. Huang, C. Yang, Z. Ju, and S.-L. Dai, "Disturbance observer enhanced variable gain controller for robot teleoperation with motion capture using wearable armbands," *Autonomous Robots*, vol. 44, no. 7, pp. 1217–1231, 2020.

[32] E. Ceseracciu, A. Mantoan, M. Bassa et al., "A flexible architecture to enhance wearable robots: integration of EMG-informed models," in *Proceedings of the 2015 IEEE/RSJ International Conference on Intelligent Robots and Systems (IROS)*, pp. 4368–4374, IEEE, Hamburg, Germany, October 2015.

[33] K. R. Saul, X. Hu, C. M. Goehler et al., "Benchmarking of dynamic simulation predictions in two software platforms using an upper limb musculoskeletal model," *Computer Methods in Biomechanics and Biomedical Engineering*, vol. 18, no. 13, pp. 1445–1458, 2015.

[34] G. Durandau, D. Farina, and M. Sartori, "Robust real-time musculoskeletal modeling driven by electromyograms," *IEEE Transactions on Biomedical Engineering*, vol. 65, no. 3, pp. 556–564, 2017.

[35] S. Yao, Y. Zhuang, Z. Li, and R. Song, "Adaptive admittance control for an ankle exoskeleton using an EMG-driven musculoskeletal model," *Frontiers in Neurorobotics*, vol. 12, p. 16, 2018.

[36] Y. Hu, Z. Li, G. Li, P. Yuan, C. Yang, and R. Song, "Development of sensory-motor fusion-based manipulation and grasping control for a robotic hand-eye system," *IEEE Transactions on Systems, Man, and Cybernetics: Systems*, vol. 47, no. 7, pp. 1169–1180, 2016.

[37] H. Huang, C. Yang, and C. P. Chen, "Optimal robot-environment interaction under broad fuzzy neural adaptive control," *IEEE Transactions on Cybernetics*, pp. 1–12, 2020.

[38] C. Yang, C. Chen, W. He, R. Cui, and Z. Li, "Robot learning system based on adaptive neural control and dynamic movement primitives," *IEEE Transactions on Neural Networks and Learning Systems*, vol. 30, no. 3, pp. 777–787, 2019.

[39] W. He, Z. Yan, C. Sun, and Y. Chen, "Adaptive neural network control of a flapping wing micro aerial vehicle with disturbance observer," *IEEE Transactions on Cybernetics*, vol. 47, no. 10, pp. 3452–3465, 2017.

[40] H. Su, J. Sandoval, P. Vieyres, G. Poisson, G. Ferrigno, and E. De Momi, "Safety-enhanced collaborative framework for tele-operated minimally invasive surgery using a 7-dof torque-controlled robot," *International Journal of Control, Automation and Systems*, vol. 16, no. 6, pp. 2915–2923, 2018.

[41] Z. Li, B. Huang, Z. Ye, M. Deng, and C. Yang, "Physical human-robot interaction of a robotic exoskeleton by admittance control," *IEEE Transactions on Industrial Electronics*, vol. 65, no. 12, pp. 9614–9624, 2018.